

Low Cycle Fatigue on Copper and Fe-Cr-Al Alloy Wires

BY

KUNTIMADDI SADANANDA

TH
me/1967/m

ME Sa15d

1967

M

SAD

LOW



DEPARTMENT OF METALLURGICAL ENGINEERING

INDIAN INSTITUTE OF TECHNOLOGY KANPUR

JULY 1967

M. Tech
173

CENTRAL LIBRARY
Indian Institute of Technology
KANPUR

Class No. *Thesis*.....

620.163

Accession No. *5a 15 L*.....

LOW CYCLE FATIGUE ON
COPPER AND Fe-Cr-Al ALLOY WIRES

by

Kuntimaddi Sadananda

In partial fulfillment of the requirements of the degree of

Master of Technology

July 1967

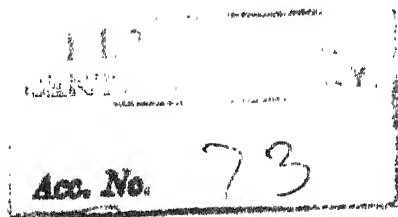


A thesis submitted to the department of

Metallurgical Engineering

of

INDIAN INSTITUTE OF TECHNOLOGY, KANPUR



600 163

83 15 1

ME-1967-M-SAD-LOW

ACKNOWLEDGEMENT

The author is indebted to Dr. M. N. Shetty for his counsel, guidance and criticism of the work in this investigation.

Grateful acknowledgement is made to National Research Council, Ottawa, for doing spectroscopic analysis of the wire samples used in this investigation.

LIST OF CONTENTS

	<u>Page</u>
I. INTRODUCTION	
1. Introduction	1
2. Stress Cycles	1
3. Internal Friction by Fatigue	2
4. Granato and Lucke - Dislocation Model	3
5. Deviations from the Theory	4
6. Purpose of the present work	6
II. EXPERIMENTAL TECHNIQUE	
1. Preparation of Specimen	7
2. Gripping Technique	8
3. Attainment and Measurement of Temperature	8
4. Measurement of Stored Energy	9
III. EXPERIMENTAL RESULTS AND DISCUSSION	
1. Experimental Procedure	9
2. Discussion	12
IV. SUMMARY AND CONCLUSION	19
V. APPENDIX	20
VI. BIBLIOGRAPHY	27

LIST OF FIGURES

- I. 1. Typical Fatigue Stress Cycle
 - (a) Reversed Stress
 - (b) Repeated Stress
 - (c) Random Stress Cycle
- I. 2. Internal Friction of Cu as a Function of Strain Amplitude and Temperature.
- I. 3. Decrement Vs Strain Amplitude
- I. 4. Granato and Lucke Dislocation Damping Model
- I. 5. Static Hysteresis
- I. 6. Granato and Lucke's Plot of Internal Friction of Cu
- I. 7. Deviations from Granato and Lucke's Analysis
- I. 8. Internal Friction of Lead as a Function of Strain Amplitude.
- II. 1. The Low Temperature Gripping Set up used for the experiment.
- III. 1. A typical Curve showing the complete sequence of Test along the Stress-strain Curve.
- III. 2. Stored energy as a function of number of cycles at constant strain-rate and pre-strain.
- III. 3. Stored energy as a function of pre-strain at constant strain rate.
- III. 4. Stored energy versus pre-strain of Steel at Constant Strain rate.
- III. 5. Stored energy versus strain rate at constant pre-strain for copper.
- III. 6. Stored energy versus strain rate at constant pre-strain for steel.
- III. 7. Activation energy plot for copper and Alloy Steel.

I. INTRODUCTION

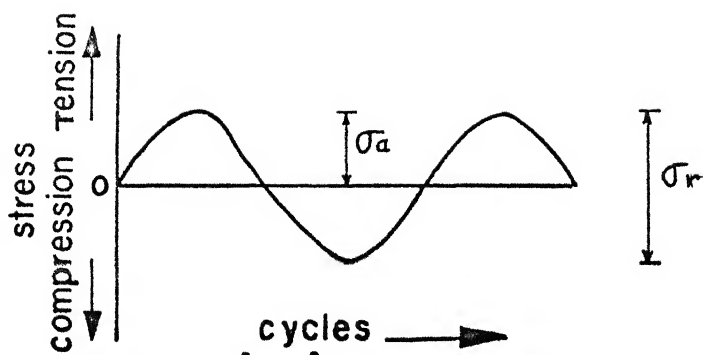
1. Introduction

It is well realized that a metal subjected to a repetitive or fluctuating stress fails at a stress much lower than that required to cause fracture on a single application of a load. Fatigue has become progressively more prevalent as technology has developed a greater amount of equipment such as automobiles, aircraft, compressors, pumps, turbines, etc., subjected to repeated loading and vibrations, and it is often stated that fatigue accounts for at least ninety per cent of all the service failures due to mechanical causes.

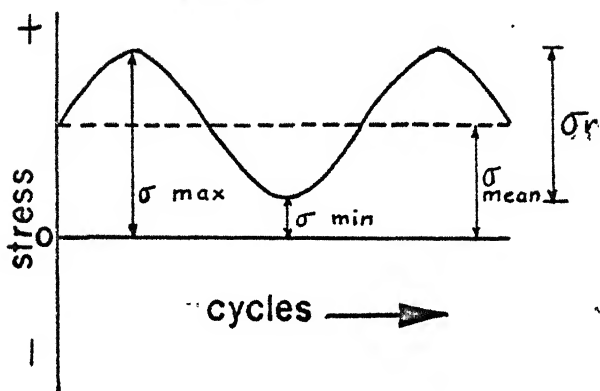
Three basic factors are to be considered for fatigue. These are (1) a maximum tensile stress, (2) a large enough fluctuation or variation in the applied stress and (3) a sufficiently large number of cycles of applied stress. A lot of other variables like stress concentration, temperature, over-load, metallurgical structure, residual stresses, etc., tend to alter the conditions for fatigue.

2. Stress Cycles

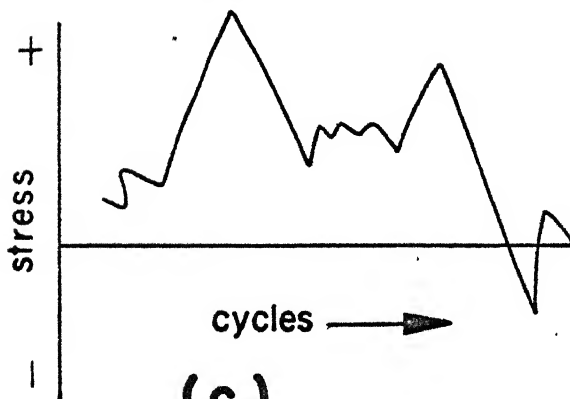
Figure I. 1 illustrates a typical fatigue stress cycle. Figure I. 1 (a) illustrates a completely reversed cycle of stress of sinusoidal form, which is an idealized situation and can be produced by a rotating beam fatigue machine. For this type of stress cycles the maximum and the minimum stresses are equal. Figure I. 1 (b) illustrates a repeated stress cycles in which the



(a)



(b)



(c)

Fig.I-1. Typical fatigue stress cycle.

(a) Reversed stress

(b) Repeated stress

(c) Random stress cycle.

maximum stress σ_{\max} and a minimum stress σ_{\min} are not equal. In this illustration they are both tensile but a repeated stress cycle could just as well contain maximum and minimum stresses of opposite signs or both in compression. In the present experiment, the σ_{\max} is a little greater than the flow stress and σ_{\min} is equal to zero. Figure I. 1 (c) illustrates a complicated stress cycle which might be encountered in a part such as an aircraft wing, which is subjected to periodic unpredictable overloads due to gusts.

Most of the fatigue data in the literature has been determined for conditions of completely reversed cycles of stress ($\sigma_{\text{mean}} = 0$). However, conditions are frequently met in engineering practice where the stress situation consists of an alternating stress and a super imposed mean stress. (Figure I. 1(c)).

Fatigue experiments are commonly used for the determination of the fatigue limit or endurance limit which can be done by plotting the "Stress vs. Number of Cycles" (S-N) curves. Hence most of the earlier experiments have been concentrated at the stress near the endurance limit which is well below the elastic limit.

I. 3. Internal Friction by Fatigue

Internal friction¹ is the capacity of the material to convert its mechanical energy of vibration into heat even when the material is thermally isolated. Internal friction corresponds to the phase lag between the applied stress and the resulting strain. The resulting strain can be resolved into elastic strain

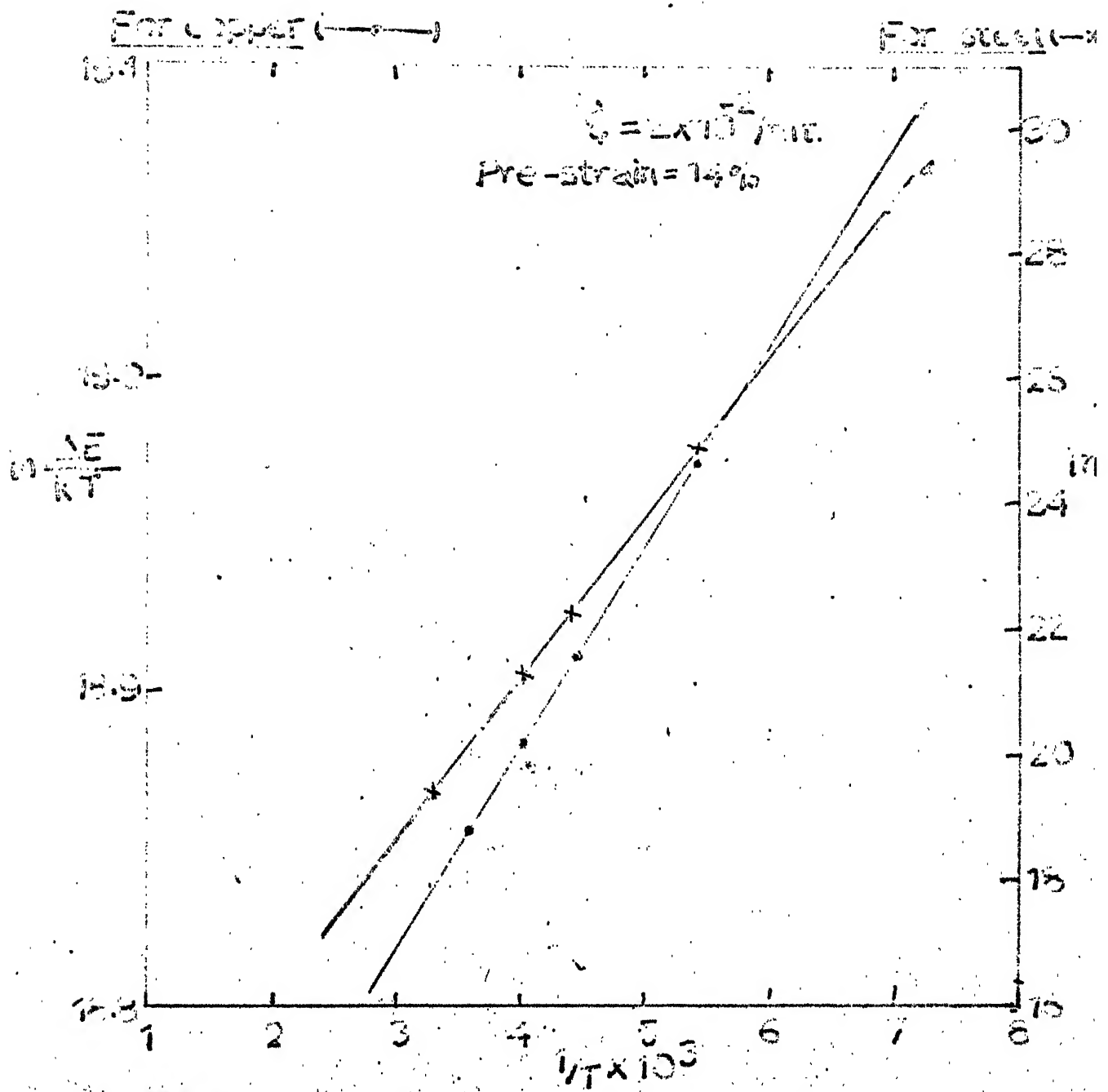


Fig. 1. Activation energy plot for copper and alloy steel.

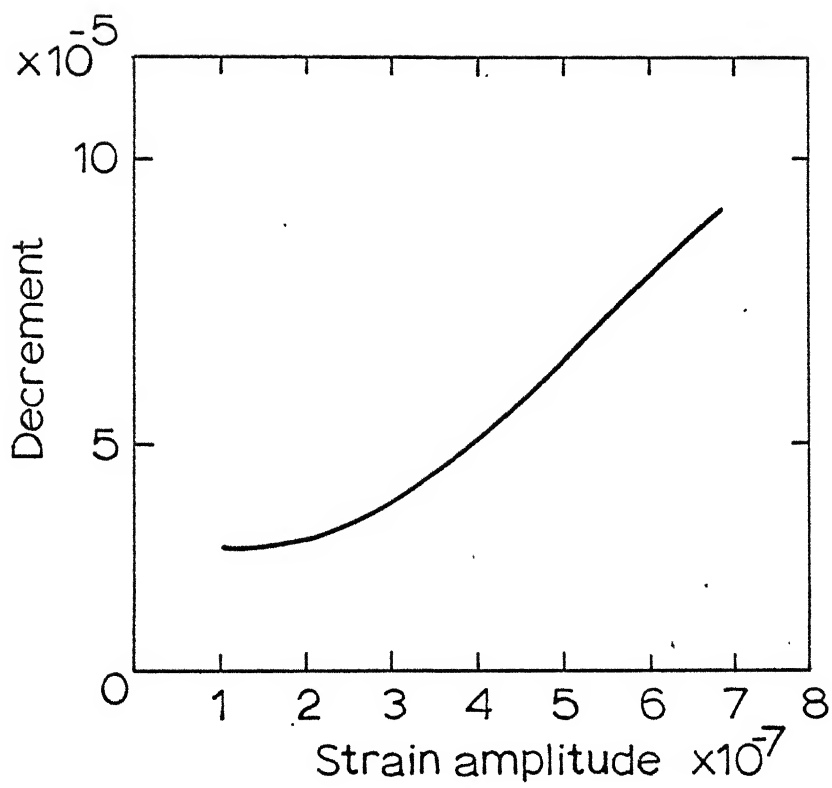


Fig. 1.3 Decrement vs. strain amplitude
(Nowick 1956)

which is in phase with the stress and anelastic strain which is out of phase with the stress. The internal rearrangement taking place to accommodate the anelastic strain is called the relaxation phenomenon.

Fatigue experiments have been extensively used to measure the internal friction² but a large body of these tests were concentrated with fatigue at low strain amplitudes, and high frequencies. In these experiments, essentially the material is subjected to fatigue at very low stresses, with the mean stress zero and at very high frequencies in the range of kilocycles.

At these low stresses, when the strain amplitude is less than 10^{-7} , internal friction is found to be independent of strain amplitude.^{3, 4} It varies linearly with strain amplitude if amplitude is greater than 10^{-7} . (Figure I. 2 and I. 3)

It is well observed⁵ that dislocations are fully responsible for amplitude-dependent internal friction and partly for amplitude-independent internal friction. A number of dislocation models⁶ have been put forth to explain the damping and of all these models the one proposed by Granato and Lucke⁷ gives a reasonably good explanation of the behavior.

I.4 Granato and Lucke - Dislocation Model

Figure I. 4 clearly gives the model of how the damping occurs in dislocations which are pinned by impurity atoms and by nodes. Figure I. 5. gives the stress-strain curve, resulting from the above model for high strain amplitudes. In this figure a, b, c and d show the motion of the dislocations

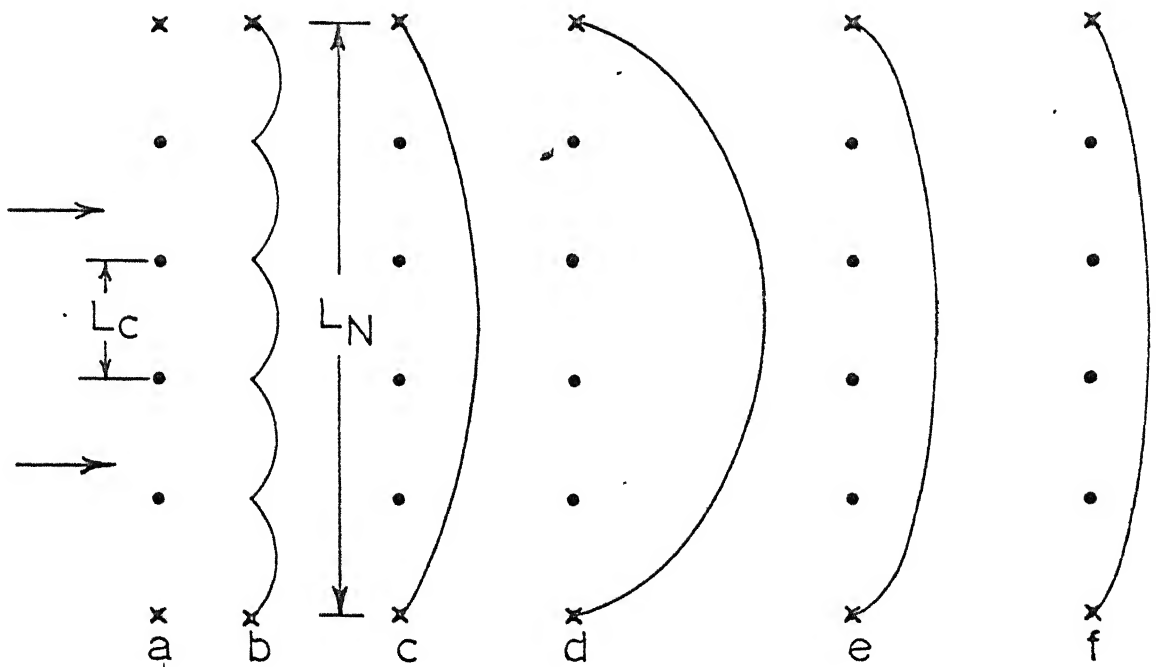


Fig. I.4 (Granato and Lucke) dislocation damping model.

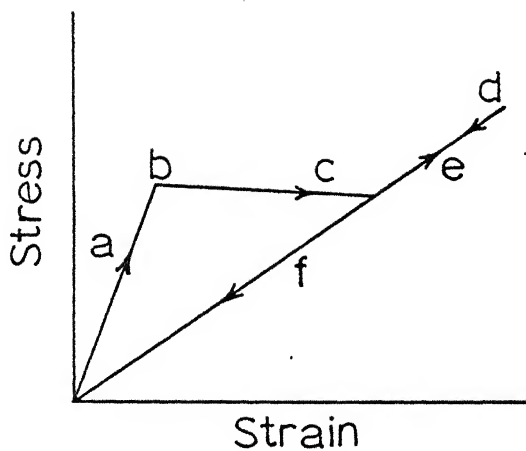


Fig. I.5 Static hysteresis (Granato and Lucke)

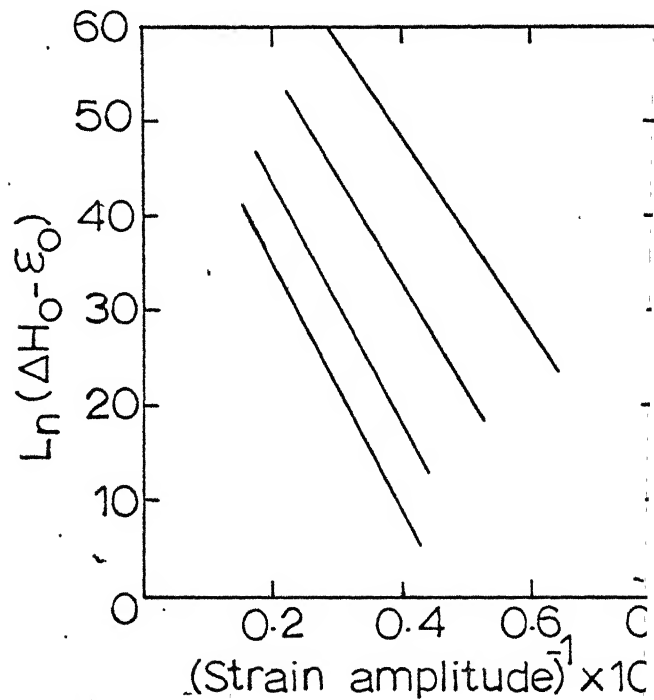


Fig. I.6 Granato and Lucke plot of internal friction c Cu- (Read 1941)

under the action of increasing stress sufficient to unpin all the impurity atoms and d, e and f show the motion as stress is decreased. Assuming an exponential distribution of dislocation segments with a length L and $L + dl$ Granato and Lucke give the following expression for the amplitude-dependent internal friction.

$$\Delta_H = \frac{\Omega \lambda L N^3 K \eta a}{\pi^2 L_c L_N E_o} \exp \left(\frac{-K \eta a}{L_a E_o} \right) \dots\dots\dots \text{Eq. I. 1.}$$

where Ω is the orientation factor. K is the factor also dependent on orientation connected with the stress required to produce unpinning, η is the Cottrell misfit parameter, a is the atomic spacing, L_c is the mean distance between impurity atoms pinned to dislocation and E_o is the maximum value of the oscillating strain.

I. 6. Deviations from the Theory

Granato and Lucke's Theory gives a fairly good account of the amplitude dependent internal friction. But recently many deviations have been observed. At high amplitudes, frequently the shape of the graph of decrement against amplitude is not reversible. Wert⁸ has shown that there is a lot of irreversibility in the amplitude-dependent internal friction.

It is found that the amplitude dependent internal friction is a function of time⁹ for which the specimen is vibrated at a high strain amplitude and of the time elapsed¹⁰ between two successive experiments. The decrement is found to decay exponentially with time.

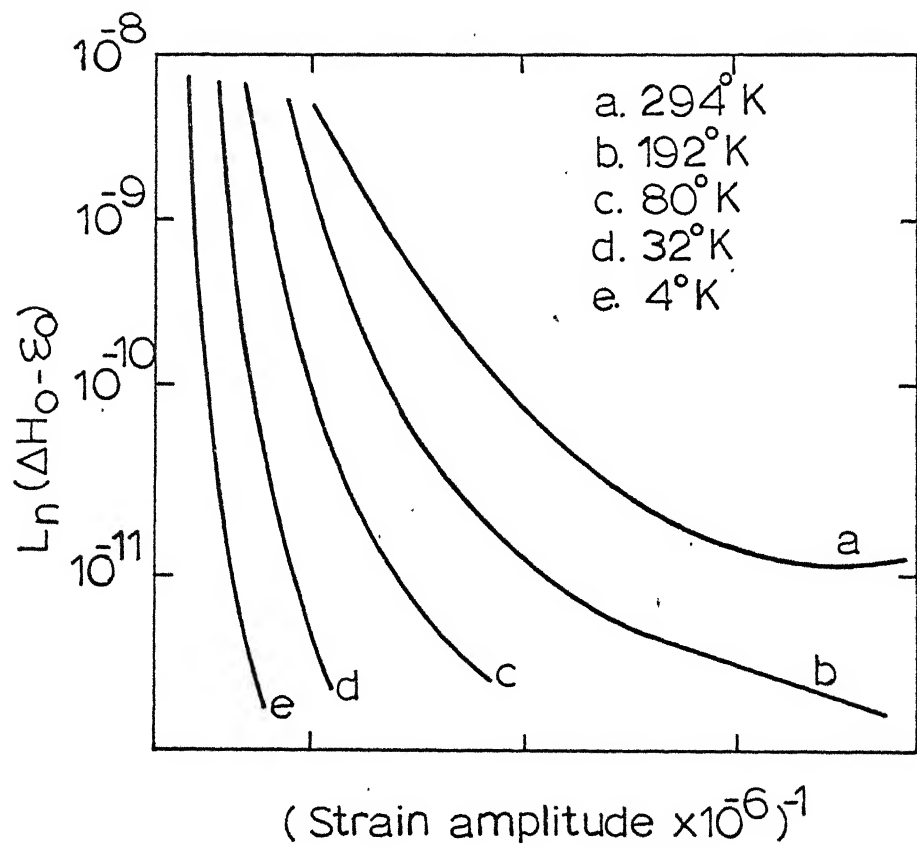


Fig.I.7. Deviations from Granato and Lucke's analysis - Caswell²⁶ (1958)

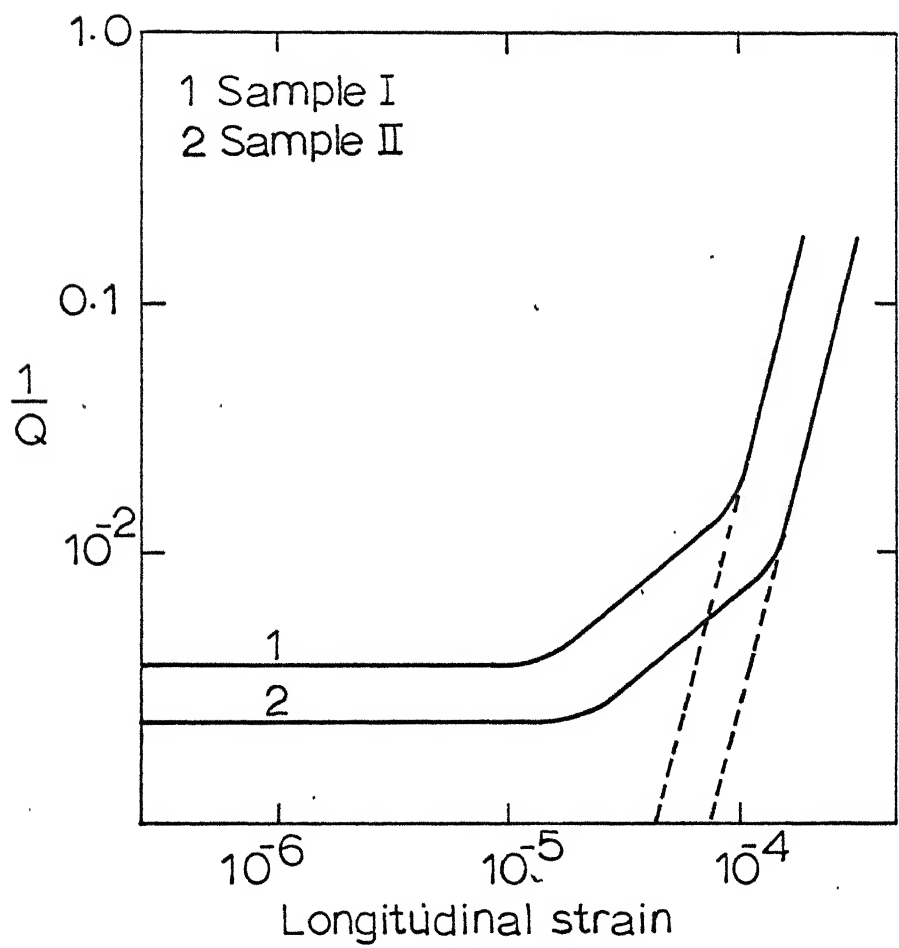


Fig. I.8 Internal friction of Lead as a function of strain amplitude (Mas on 1956)

$$(\Delta - \Delta_0) = (\Delta_I - \Delta_0) \exp(-Bt)^\eta \dots \dots \dots \text{Eq I. 2.}$$

where Δ_0 is the initial decrement, Δ_I is the maximum decrement, t is the time after the end of excitation period and η is found to be a function of time.

Granato and Lucke¹¹ analyze Reed's¹² results and find a linear relationship (Figure I-7) between $\ln(\Delta H \cdot E_0)$ and $1/E_0$ as predicted by the equation I-1. But a non-linear relationship is observed by Caswell⁴ and Nowick¹³ for copper at high strain amplitudes.

The only effect of temperature considered by the model is the equilibrium concentration of impurity atoms on dislocations as given by Cottrell.¹⁴ The effect of thermal energy at higher temperatures is to aid the dislocations as it attempts to break away from the pinning points and this has been neglected.

The effect of frequency is also not clear as the observations have been varied. Nowick¹³ observes decrement to be independent of frequency as predicted by the model, whereas Kamensky¹⁵ observes that decrement in copper single crystals increases with frequency. But in all these experiments the strain amplitude is not very high.

Mason¹⁶ measured decrement as a function of strain amplitude and found three regions (Figure I-8); (1) region below 10^{-5} where the decrement is independent of strain amplitude, (2) region between 10^{-5} and 10^{-4} where the decrement increases with increasing amplitude in a reversible manner, and (3) region above 10^{-4} where the decrement increases very rapidly and irreversibly.

It is very clear that Granato and Lucke's model fails to give a satisfactory explanation for the amplitudes greater than the break-away amplitude. Mason¹⁶ and Baker¹⁷ performed experiments at strain cycles of 10^{-3} . However, sufficient experimental material at high strains is not available to understand the mechanism of relaxation. Reed, Hill¹⁸ et al. pre-strained zirconium at 77° K and subjected it to high amplitude fatigue at room temperature. They observed that the pre-straining at 77° K resulted in the formation of large numbers of stable deformation twins $(11\bar{2}1)$. These twins caused a large room temperature mechanical hysteresis when the material was under cyclic tensile loading. They observed that hysteresis was maximum when the prestrain was just under 1%. It also depended strongly on the maximum applied cyclic stress, but only moderately on the loading rate and temperature. The observed anelastic phenomena was explained on the assumption that they are the results of stress induced twin boundary movements in which the average twin increases its thickness by only a few per cent. But this relaxation mechanism may not be valid for other materials. Each material has to be tested and the relaxation mechanism has to be determined on its own merit.

I. 7. Purpose of the Present Work

The present work is intended to observe the fatigue behavior of copper and an alloy steel at very high stresses and very low frequencies with the mean stress greater than zero. Copper has been chosen in the present work because extensive work has been done on this material and the information obtained

by several investigators shows that the data are not consistent with Granato and Lucke model. Virtually no information is available on the alloy used in this work. Since the Granato and Lucke model is found to be unsatisfactory it is hoped that the activation energies obtained by studying the temperature dependence of stored energy would enable an understanding of the rate controlling mechanism of the relaxation process. In regular fatigue experiments, it is somewhat difficult to make any energy measurements and it is hoped that the present experiments on low cycle fatigue would do this and bridge the gap between regular internal friction and fatigue experiments.

II. EXPERIMENTAL TECHNIQUE

II. 1. Preparation of the Specimen

High amplitude low cycle fatigue experiments are performed on conductivity grade copper and an alloy of iron-chromium-aluminum. The copper and the alloy specimens are in the form of wires of cross-sectional area 0.00028 sq. cm. and 0.00164 sq. cm. respectively. Both are cut to a length of 5 cm. The spectroscopic analysis as given by the National Research council, Ottawa, Canada is as follows:

<u>Copper Specimen</u>		<u>Alloy Steel</u>	
Pb	-0.001 %	Cr	-10 %
Sn	-0.001 %	Al	- 5 %
Fe	-0.005 %	Mn	- 2 %
Ni	-0.0001 %	Si	- 2 %
Bi	-0.0001 %	Ni	- 1 %
Ag	-0.0005 %	V	- 0.1 %
Mg	-Trace	Mg	- 0.01 %
		C	- 0.02 %
		Mo, Ca, Co	- Trace

The wire specimens are first stress annealed in nitrogen atmosphere at 300° C for half an hour.

II. 2. Gripping Technique

The specimens are subjected to cyclic loading in an Instron tensile testing machine. Figure II-1 represents schematically the grips employed for the experiments. The whole assembly is aligned properly. The wire grips are so designed that they can be used only in tension. Hence in these experiments the mean stress is greater than zero.

II. 3. Attainment and Measurement of Temperature

Different temperatures are obtained by using freezing mixtures.¹⁹

The whole assembly including the grips are immersed in the freezing mixture, contained in a big Dewar flask. The duration of the experiment is three to

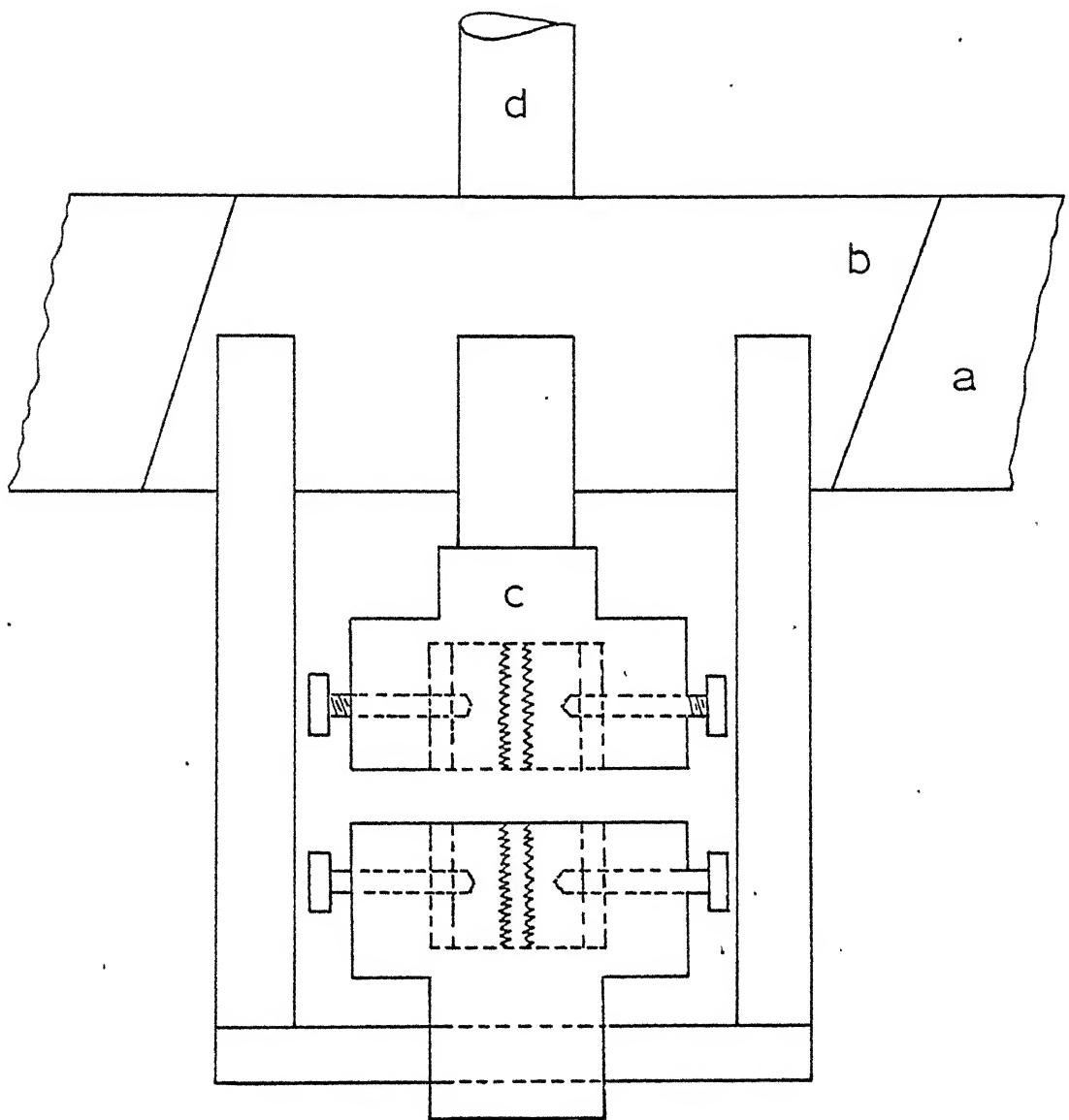


Fig. II.1 The low-temperature gripping set-up used for the experiment.

- a. Instron anvil b. Brass plate c. Brass vessel
d. Mild steel rod thru which load is transferred thru load cell.

four hours and throughout this time the temperature is maintained fairly constant. The maximum variation of temperature after three hours is 2 to 3° C. Table II-1 gives different baths employed to attain different temperatures.

TABLE II-1

<u>S. No.</u>	<u>Bath Composition</u>	<u>Temperature</u>
1	Acetone	-94° C
2	Ethyl alcohol + 15% water (by vol.)	-50° C
3	Ethyl alcohol + 25% water (by vol.)	-30° C
4	Ice-water	0° C
5	Room temperature	27° C

The baths are frozen by passing liquid nitrogen. The temperatures are measured with a copper constantan thermocouple.

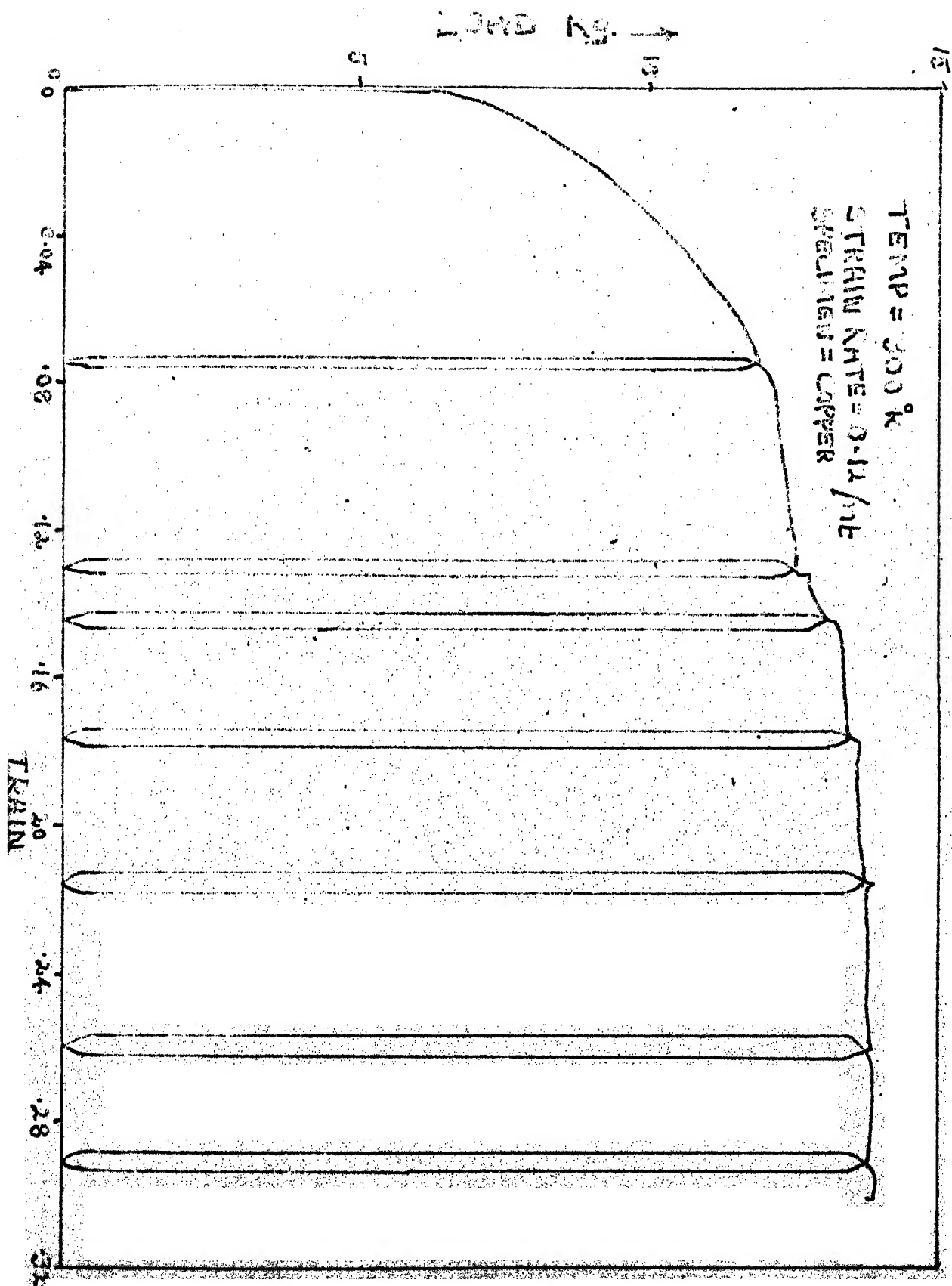
II. 4. Measurement of Stored Energy

Stored energy in each cycle is measured by using the integrator, a planometer attachment supplied by the Instron Company. The maximum error in integration by integrator is of the order of 1%.

III. EXPERIMENTAL RESULTS AND DISCUSSION

III. 1. Experimental Procedure

The wire is taken along the stress-strain curve to a value of the stress ($\overline{\sigma}_{\max}$), very close to the flow stress of the material, and is subjected to fatigue between zero and $\overline{\sigma}_{\max}$. A typical stress-strain curve during the



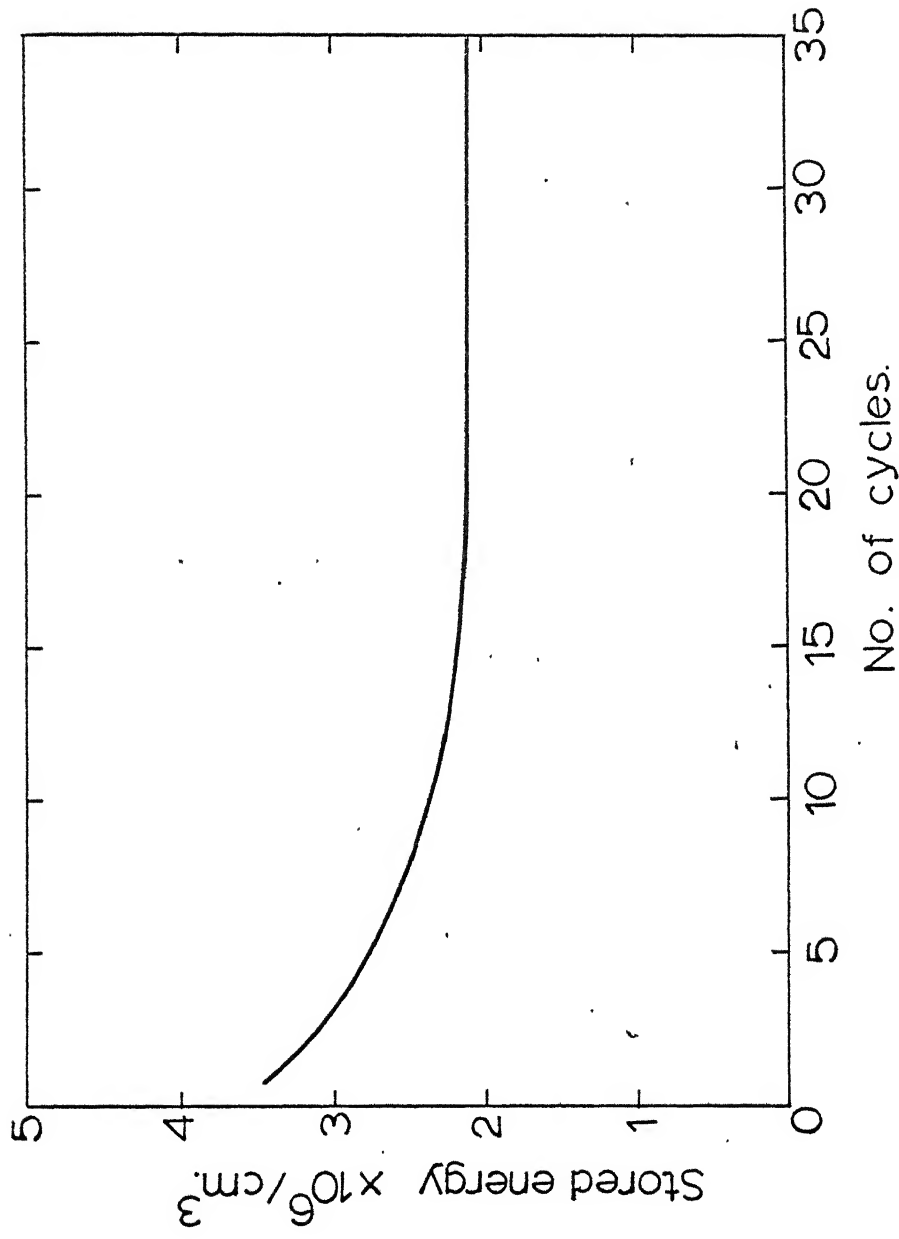


Fig. III.2 - Stored energy as a function of no. of cycles at constant strain rate and pre-strain.

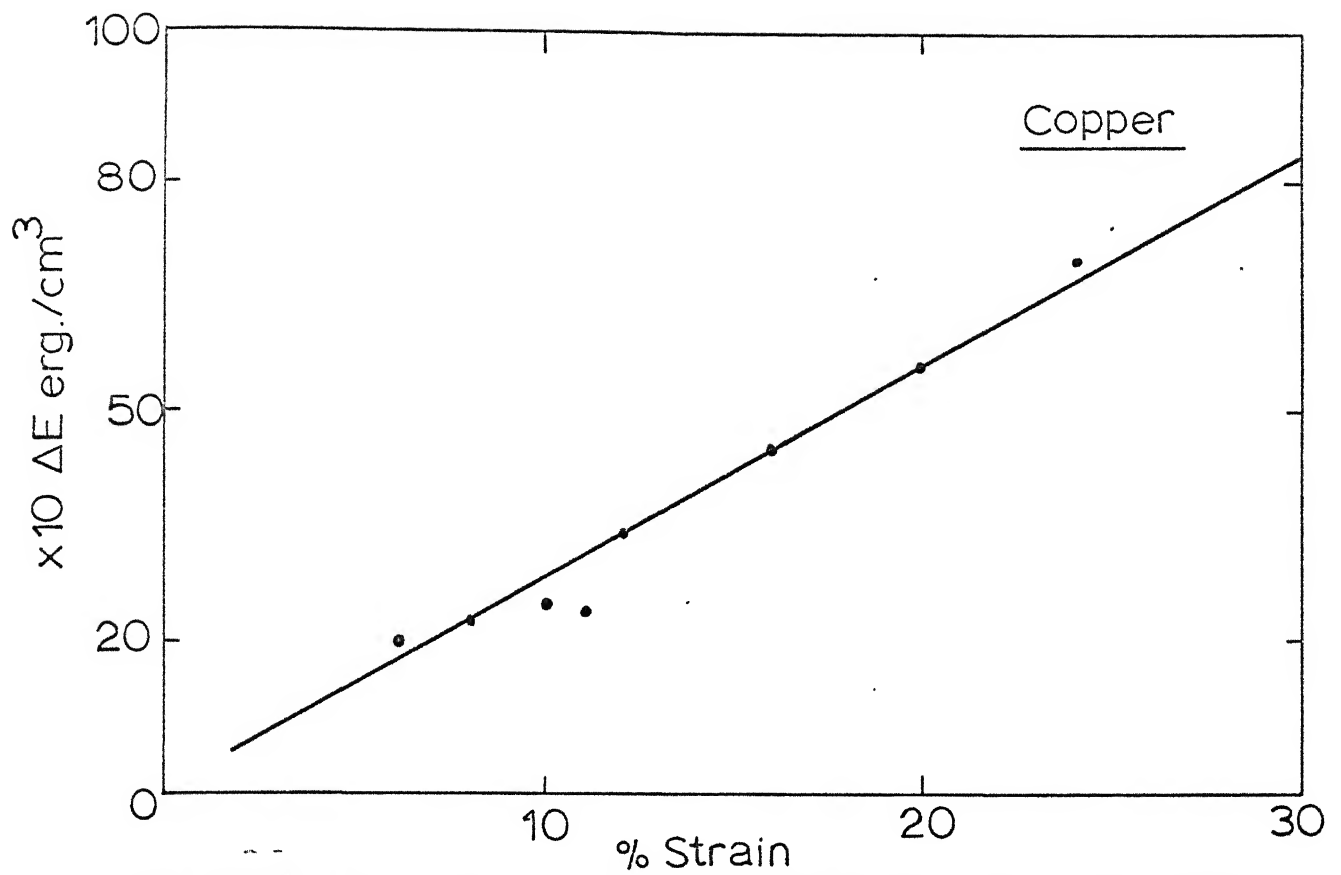


Fig. III.3 - Stored energy as a function of Pre-strain at Constant Strain rate (0.01cm/mt)

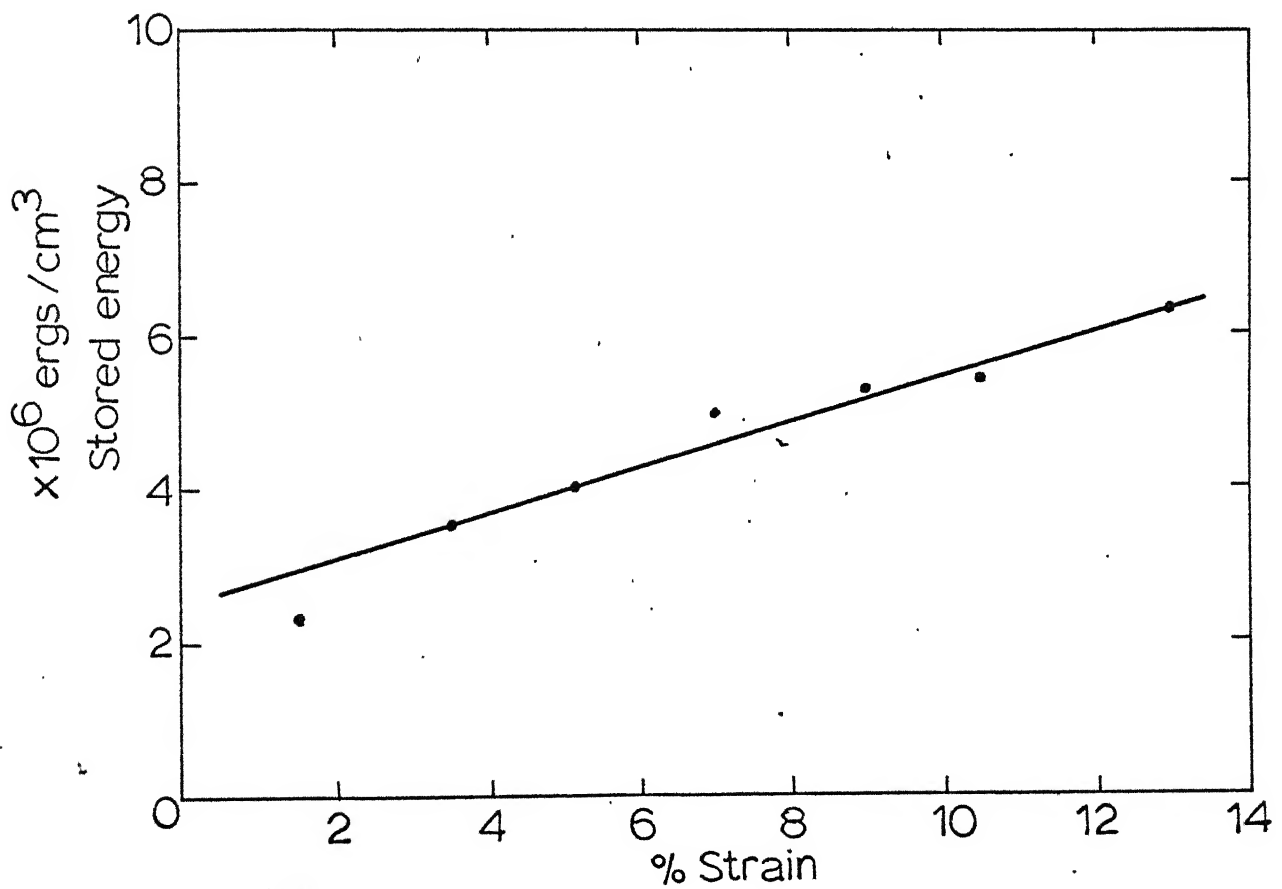


Fig. III.4 - Stored energy vs Pre-strain of steel at

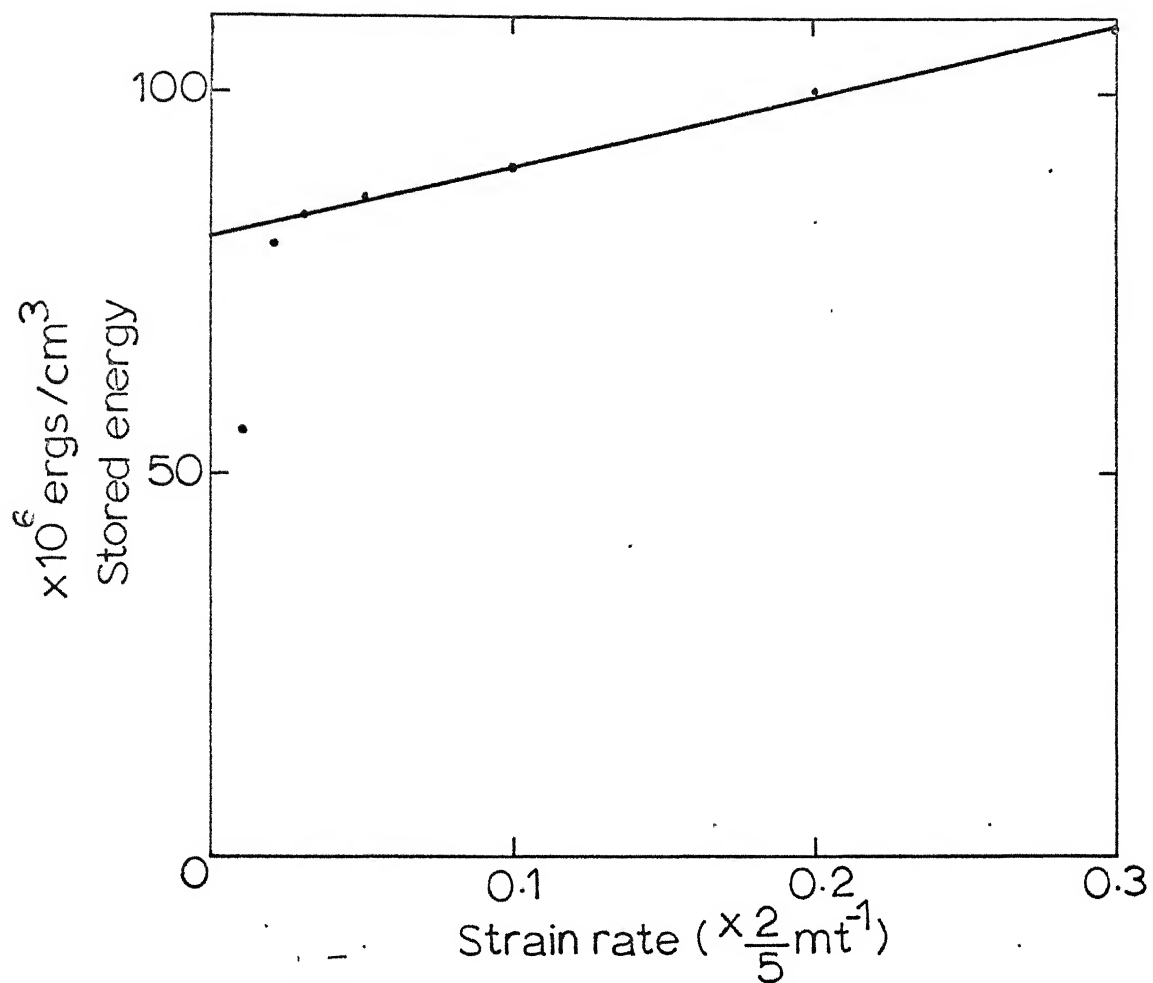


Fig III.5 Stored energy vs. Strain rate at constant Pre-strain for copper.

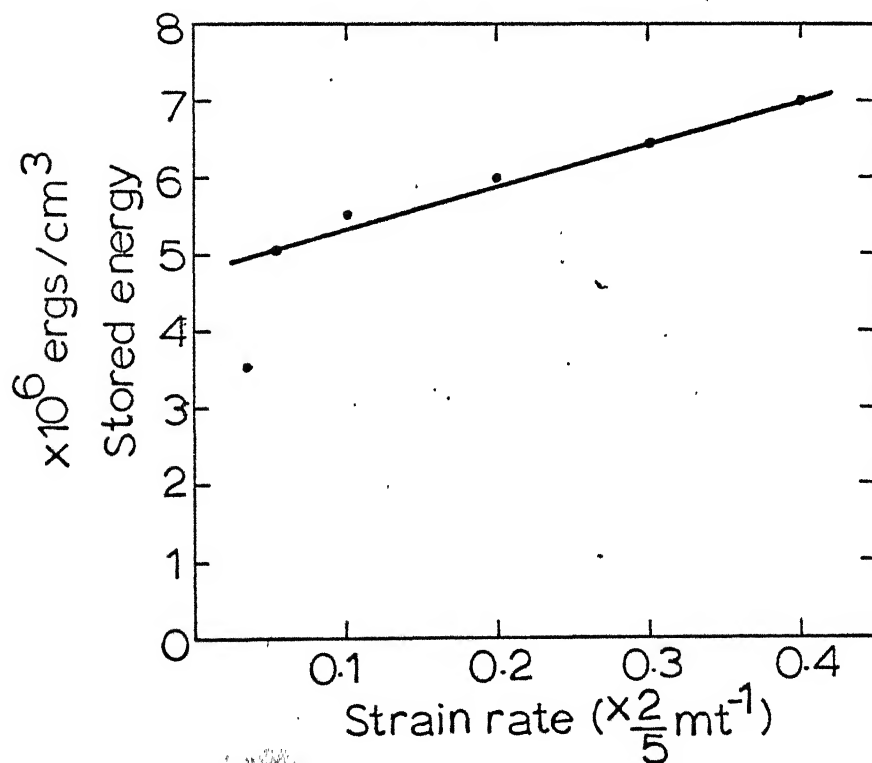


Fig III.6 Stored energy vs. Strain rate at _____

cyclic loading is shown in Figure III-1 which also shows the energy stored during the first few cycles in the sample. The stored energy is measured as a function of the number of cycles. The Figure III-2 shows the effect of the number of cycles on the stored energy per cycle. The energy decreases rapidly for the first few cycles and becomes constant after sufficient number of cycles. The constant energy thus obtained from the curve is recorded.

The specimen is next taken to a higher value of the strain all along the stress strain curve and again subjected to fatigue between zero and σ_{\max} . The stored energy is measured as a function of the number of cycles. The energy decreases rapidly for the first few cycles and becomes constant after sufficient number of cycles. This constant energy is recorded. The material is then taken to a higher value of strain and the whole process is repeated to get constant energy as a function of the number of cycles. The experiment is repeated for different strains all along the stress strain curve. Figure III-2(b) is a typical curve showing the complete sequency of operation for copper along the stress strain curve. The constant stored energy obtained as a function of t number of cycles at each strain is plotted as a function of Pre-Strain. During this experiment the strain rate and temperature are kept fairly constant. Figure III-3 and III-4 show the effect of prestrain on the stored energy per cycle at 0.01/2.5 strain rate and at 300° K for copper and alloy respectively.

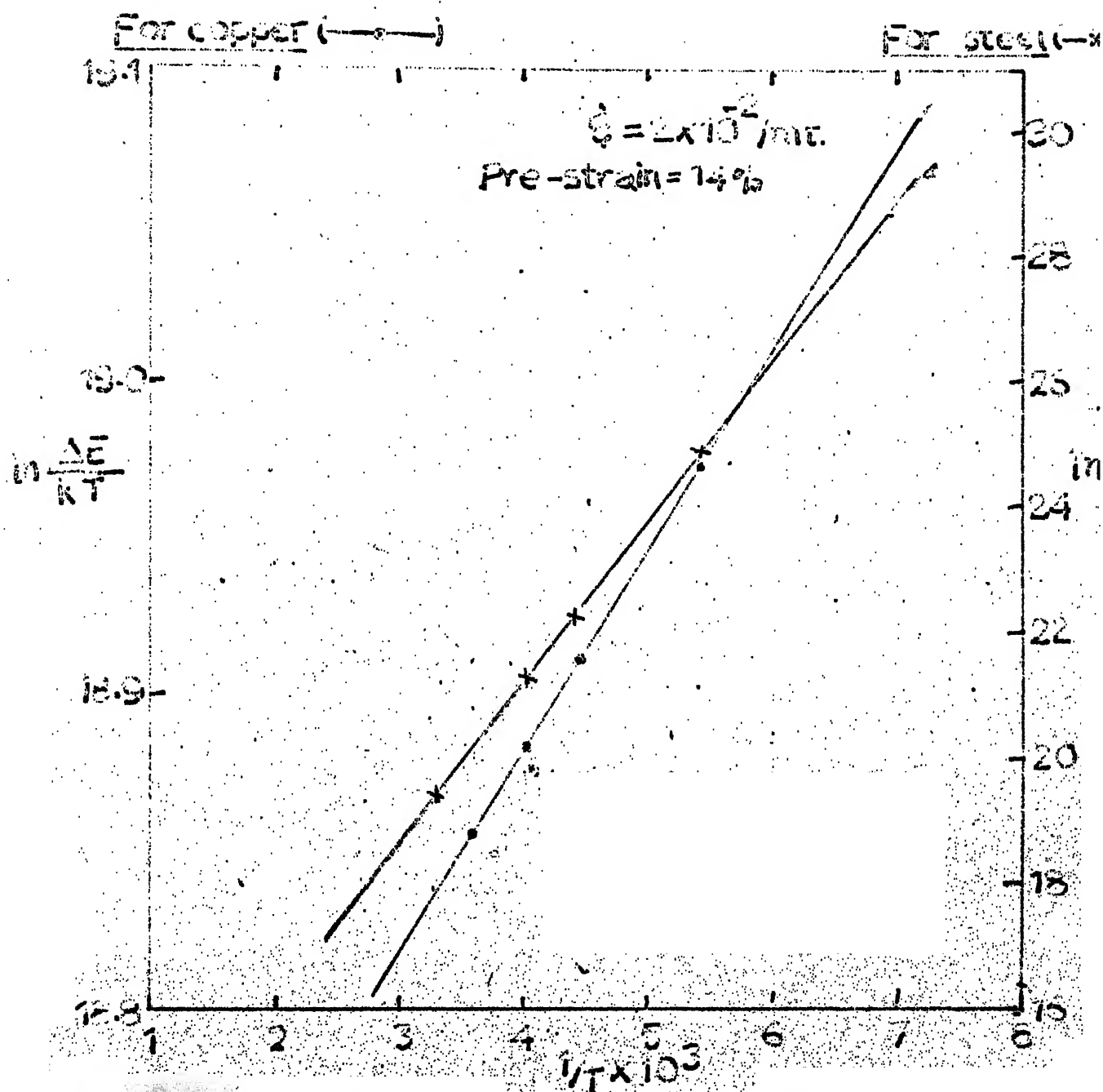


Fig. III.7 Activation energy plot for copper and alloy steel

Each time strain rate is varied and for each strain rate the stored energy as a function of prestrain is determined. The data in the appendix - A show the effect of prestrain on stored energy for different strain rates. From this data, the effect of strain rate on the stored energy at constant prestrain is determined. Figure III-5 and III-6 show the effect of strain rate at room temperature for copper and alloy respectively. Stored energy increases linearly with strain rate for both copper and alloy.

For one strain rate, the experiment is repeated at different temperatures. Appendix B shows the effect of temperature on $\ln \frac{\Delta E}{kT}$, where ΔE is the stored energy per cycle and kT is the thermal energy for different prestrains. Using this data, $\ln \frac{\Delta E}{kT}$ against $\frac{1}{T}$ is plotted to determine the activation energy of the rate controlling mechanism (Figure III-7). The slopes of these curves give the activation energy.

In all these experiments all the tests where the specimen failed at the grips have been rejected and only those where the specimen failed at the center have been recorded. In this way it is expected to keep the grips effects to a minimum.

The experiments are somewhat similar to that of Reed-Hill, et al. who worked on zirconium at room temperature. The main difference is that they prestrained zirconium at 77° K. This prestraining at low temperature stabilized the deformation twins that are produced, which caused anelasticity at room temperature.

Each time strain rate is varied and for each strain rate the stored energy as a function of prestrain is determined. The data in the appendix - A show the effect of prestrain on stored energy for different strain rates. From this data, the effect of strain rate on the stored energy at constant prestrain is determined. Figure III-5 and III-6 show the effect of strain rate at room temperature for copper and alloy respectively. Stored energy increases linearly with strain rate for both copper and alloy.

For one strain rate, the experiment is repeated at different temperatures. Appendix B shows the effect of temperature on $\ln \frac{\Delta E}{kT}$, where ΔE is the stored energy per cycle and kT is the thermal energy for different prestrains. Using this data, $\ln \frac{\Delta E}{kT}$ against $\frac{1}{T}$ is plotted to determine the activation energy of the rate controlling mechanism (Figure III-7). The slopes of these curves give the activation energy.

In all these experiments all the tests where the specimen failed at the grips have been rejected and only those where the specimen failed at the center have been recorded. In this way it is expected to keep the grips effects to a minimum.

The experiments are somewhat similar to that of Reed-Hill, et al. who worked on zirconium at room temperature. The main difference is that they prestrained zirconium at 77° K. This prestraining at low temperature stabilized the deformation twins that are produced, which caused anelasticity at room temperature.

III. 2. Discussion

From the stored energy in each cycle, internal friction can be calculated by using the formula

$$\Delta = \frac{\Delta W}{2 W} = \frac{\Delta W}{\sigma_{\max}^2} / G \dots\dots\dots \text{Eq III-1}$$

where Δ is the decrement, ΔW is the energy stored in each cycle, σ_{\max} is the maximum stress and G is the rigidity modulus. Though the above equation is used for the cycle with the mean stress zero, even otherwise, the decrement is proportional to the stored energy. The variation of stored energy as a function of the number of cycles, Figure III-2 is similar to the variation of the decrement as a function of time, at high strain amplitudes. Even in this case, the exponential equation can be said to be valid. Reed-Hill, et al. obtained similar curves for zirconium.

Figures III-5 and III-6 show that stored energy is linearly related to strain rate in support of the observations of Kamensky and thereby contradicting the Granato and Lucke model. The proportionality of the stored energy to strain rate clearly shows that there is certain relaxation phenomenon that is taking place in the material even at this high strain. To explain this, the following analysis is done.

The energy stored in each hysteresis cycle can be computed from the stress strain curve and is given by

$$\Delta E = \int_0^{\sigma_{\max}} \sigma dE_f - \int_{\sigma_{\max}}^0 \sigma dE_r \dots\dots\dots \text{Eq. III-}$$

where dE_f is the strain increment during forward motion and dE_r is the strain decrement during reverse motion.

These can be obtained from the stress strain equation

$$\dot{E} = NAG \nu \exp - \left[\frac{U_0 - V(\bar{\sigma}_m \pm \bar{\sigma}_i)}{KT} \right] \dots\dots\dots \text{Eq. III-3}$$

where \dot{E} = strain rate; $NAG = E$, the strain; N = the number of activated dislocations; A - area they sweep through; b = the larger vector of the dislocations; U = the activation energy; V = the activation volume; $\bar{\sigma}_m$ = the applied maximum stress; $\bar{\sigma}_i$ = the internal stress and ν = Debye frequency.

For forward and backward motions the equation reduces to

$$\dot{E}_f = E_f \nu \exp - \left[\frac{U_0 - V(\bar{\sigma}_m - \bar{\sigma}_i)}{KT} \right] \dots\dots\dots \text{Eq. III-4}$$

and

$$\dot{E}_r = E_r \nu \exp - \left[\frac{U_0 - V(\bar{\sigma}_m + \bar{\sigma}_i)}{KT} \right] \dots\dots\dots \text{Eq. III-5}$$

differentiating with respect to the strain, we have

$$dE_f = \frac{\dot{E}_f}{\nu} e^{\frac{U_0}{KT}} e^{\frac{-V(\bar{\sigma}_m - \bar{\sigma}_i)}{KT}} \cdot \left(\frac{-V}{KT} \right) d\bar{\sigma} \dots\dots \text{Eq. III-6}$$

$$dE_r = \frac{\dot{E}_r}{\nu} e^{\frac{U_0}{KT}} e^{\frac{-V(\bar{\sigma}_m + \bar{\sigma}_i)}{KT}} \cdot \left(\frac{-V}{KT} \right) d\bar{\sigma} \dots\dots \text{Eq. III-7}$$

The strain rate is kept fairly constant throughout the cycle. Hence

$$\dot{E}_f \approx \dot{E}_r \approx \dot{E} \dots\dots\dots \text{Eq. III-8}$$

From equations III-2, III-6 and III-7, the stored energy in each cycle is given by

$$\Delta E = \frac{-V}{KT} \frac{E_f}{\sqrt{}} \int_0^{\sqrt{\max}} e^{\frac{U_0 - V(\sqrt{} - \sqrt{i})}{KT}} d\sqrt{} - \left(\frac{-V}{KT} \right) \frac{E_r}{\sqrt{}} \int_{\sqrt{\max}}^0 e^{\frac{U_0 - V(\sqrt{} + \sqrt{i})}{KT}} d\sqrt{} \dots \text{Eq. III-9}$$

By equation III-8, the above equation reduces to

$$\Delta E = \frac{-VE}{KT\sqrt{}} \int_0^{\sqrt{\max}} e^{\frac{U_0 - V(\sqrt{} - \sqrt{i})}{KT}} d\sqrt{} + \left(\frac{-V}{KT} \right) \frac{E}{\sqrt{}} \int_0^{\sqrt{\max}} e^{\frac{U_0 - V(\sqrt{} - \sqrt{i})}{KT}} d\sqrt{} \dots \text{Eq. III-10}$$

This on integration by parts gives

$$\Delta E = \frac{E}{\sqrt{}} e^{\frac{U_0}{KT}} \left\{ \left[e^{\frac{-V(\sqrt{} - \sqrt{i})}{KT}} - e^{\frac{-V(\sqrt{} - \sqrt{i})}{KT}} \right] - \left[\int_0^{\sqrt{\max}} e^{\frac{-V(\sqrt{} - \sqrt{i})}{KT}} - e^{\frac{-V(\sqrt{} + \sqrt{i})}{KT}} \right] \right\}$$

$$\Delta E = \frac{\dot{E}}{\dot{\gamma}} e^{\frac{U_0}{KT}} \left[\dot{\gamma} \left(e^{\frac{-V(\sqrt{\sigma}_m - \sqrt{\sigma}_i)}{KT}} - e^{\frac{-V(\sqrt{\sigma}_m + \sqrt{\sigma}_i)}{KT}} \right) - \frac{KT}{V} \left[e^{\frac{-V(\sqrt{\sigma}_m - \sqrt{\sigma}_i)}{KT}} - e^{\frac{-V(\sqrt{\sigma}_m + \sqrt{\sigma}_i)}{KT}} \right] \right] \text{Eq. III-11}$$

$$\Delta E = \frac{\dot{E}}{\dot{\gamma}} e^{\frac{U_0}{KT}} \left(\dot{\gamma} + \frac{KT}{V} \right) \left[e^{\frac{-V(\sqrt{\sigma}_m - \sqrt{\sigma}_i)}{KT}} - e^{\frac{-V(\sqrt{\sigma}_m + \sqrt{\sigma}_i)}{KT}} \right] \text{Eq. III-12}$$

At very high strain amplitudes of the order of 10^{-2} to 10^{-1} , the internal stress which is mainly due to the fewest dislocations may be of the order of $\sqrt{\sigma}_{max}$; under this approximation the above equation reduces to

$$\Delta E = \frac{\dot{E}}{\dot{\gamma}} \frac{1}{KT} \left(\frac{\sqrt{\sigma}_m}{KT} + \frac{1}{V} \right) e^{\frac{U_0 - 2V\sqrt{\sigma}_m}{KT}} \text{Eq. III-13}$$

Assuming that $\sqrt{\sigma}_m$ varies linearly with temperature and V the effective volume is independent of temperature, the pre-exponential factor of temperature is eliminated by division. Then the equation is

$$\frac{\Delta E}{KT} = \frac{\dot{E}}{\dot{\gamma}} \left(\frac{\sqrt{\sigma}_m}{KT} + \frac{1}{V} \right) e^{\frac{U_0 - 2V\sqrt{\sigma}_m}{KT}} \text{Eq. III-14}$$

and

$$\ln \frac{\Delta E}{KT} = \frac{U_0 - 2V\sqrt{\sigma}_m}{KT} + \ln \left[\frac{\dot{E}}{\dot{\gamma}} \left(\frac{\sqrt{\sigma}_m}{KT} + \frac{1}{V} \right) \right] \text{Eq. III-14}$$

Equation III-14 can be used to plot $\ln \frac{\dot{A}E}{KT}$ vs $1/T$. (Figure III-7).

The slope of the curve gives $\frac{U_0 - 2V \sqrt{\tau_m}}{K}$.

The activation volume V is determined by using the equation given below which follows from equation III-2.

$$V = \frac{KT \ln \frac{\dot{E}_1}{\dot{E}_2}}{\tau_1 - \tau_2}$$

where τ_1 and τ_2 are flow stresses of the material at strain rates \dot{E}_1 and \dot{E}_2 . So as to determine the value of V , the material is stressed at different strain rates and the flow stress at each strain rate is measured from the stress strain curve. Substituting the values of flow stress at different strain rates and also the corresponding strain rates into the equation, the activated volume is calculated. The average value of the activation volume for copper and alloy is 1.7×10^{-22} and $1.5 \times 10^{-22} \text{ cm}^3$ respectively.

The values of $\frac{U_0 - 2V \sqrt{\tau_m}}{K}$ as given from the slope of the curve III-7 for copper and alloy are 64 and 56 respectively. The activation energies determined in this way are found to be about 0.5 ev for both copper and alloy steel.

The dependency of stored energy strain rate (Figures III-5 and III-6) shows that there is certain relaxation taking place in the material even at this high strain amplitude.

Mason suggested that rapid increase in internal friction at high strain amplitudes was probably due to the dislocation loops cutting through the pinning dislocations and producing jogs, vacancies, etc.

Birnbaum²⁰ and Levy calculated the activation energy for the formation of a vacancy or interstitial at the dislocation intersections and they indicate that it is of the order of 0.5 to 0.7 ev. for Aluminium. Hirsh²¹ gives the same order of magnitude for copper. According to Hirsh, this can be easily seen as follows. Elementary jogs of one burger vector length, formed by the intersection of forest dislocations can be considered as short dislocations normal to slip planes and equal in length to that of spacing between them, plus kinks lying in the slip planes. These jogs can disassociate to form an extended jog which is essentially a line defect.

These low energy jog lines can move side ways by a mechanism in which atoms jump to their neighboring positions; this motion starting at one of the two partials of the ribbon. During this process a partial or full vacancy or interstitial is created at the jog partial depending upon the direction of motion. For the creation of partial or full vacancies the activation energy required is less than that of vacancy diffusion, i.e., less than 0.8 ev. for copper as given by Hirsh which is an approximate value. For iron too it is of the order of 0.9 ev. but due to the presence of substitutional elements like chromium, aluminium, the formation energy of a vacancy may be less than that in pure iron. For the creation of interstitial a higher energy is required.

From the magnitude of the activation energy obtained in the present work, it is postulated that one of the possible mechanisms of relaxation may be due to the formation of a vacancy at the extended jogs of screw dislocation. It is known that as the strain increases a large number of dislocations can intersect producing jogs and vacancies. Therefore, our observation that stored energy increases with increasing prestrain appears to be consistent with the vacancy mechanism.

IV. SUMMARY AND CONCLUSION

Each cycle, high amplitude fatigue measurements are made on copper and alloy steel wires. The effect of the number of cycles, prestrain, strain rate and temperature on stored energy in each cycle has been determined. The stored energy is found to

- 1.) reach a stable value as a function of the number of cycles
- 2.) increase linearly with strain rate
- 3.) increase linearly with prestrain.

Using low temperature data, the activation energy is determined. From the activation energy measurements it is suggested that a possible mechanism may be the formation of a vacancy at the extended elementary jogs of screw dislocations.

The precision in the above experiments is limited to a number of uncontrollable factors. Apart from the assumption used in determining the activation energy, the accuracy in the measurements is also effected by the size of the specimens. But the wire specimens are particularly selected to minimize the errors due to the relaxation of the instrument.

Therefore, no definite conclusions concerning the exact mechanism of relaxation can be reached until further work is done on different materials in this field.

V. APPENDIX

Appendix A

Room Temperature Readings for Copper

1. Strain rate $\frac{0.05}{2.5}$ / mt.

<u>S. No.</u>	<u>Pre-Strain</u>	<u>Stored energy x 10 ergs/cm³</u>
1	0.0482	10.2
2	0.0762	13.2
3	0.1002	41.8
4	0.1016	42
5	0.1354	54.2
6	0.1570	64.8
7	0.1790	83.8
8	0.1934	71
9	0.231	102

2. Strain rate $\frac{0.005}{2.5}$ / mt.

<u>S. No.</u>	<u>Pre-Strain</u>	<u>Stored energy x 10 ergs/cm³</u>
1	0.017	2.9
2	0.039	12
3	0.067	20.9
4	0.100	42
5	0.134	91
6	0.167	97.5

3. Strain rate $\frac{0.01}{2.5}$ / mt.

<u>S. No.</u>	<u>Pre-Strain</u>	<u>Stored energy x 10 ergs/cm³</u>
1	0.0068	4.18
2	0.0122	5.00
3	0.023	6.29
4	0.0418	16.7
5	0.0552	26.25
6	0.0684	34.0
7	0.083	59
8	0.1000	41
9	0.1244	36.7

4. Strain rate $\frac{0.02}{2.5}$ / mt.

<u>S. No.</u>	<u>Pre-Strain</u>	<u>Stored energy x 10 ergs/cm³</u>
1	0.0447	13.4
2	0.085	30.0
3	0.113	43.5
4	0.138	132.0
5	0.154	66.9

5. Strain rate $\frac{0.03}{2.5}$ / mt.

<u>S. No.</u>	<u>Pre-Strain</u>	<u>Stored energy x 10 ergs/cm³</u>
1	0.0385	11.22
2	0.0635	21.25
3	0.09	23.8
4	0.115	42.6
5	0.152	75.2
6	0.181	80.0
7	0.217	95.4
8	0.267	101.5

6. Strain rate $\frac{0.2}{2.5}$ / mt.

<u>S. No.</u>	<u>Pre-Strain</u>	<u>Stored energy x 10 ergs/cm³</u>
1	0.008	4.18
2	0.0232	6.3
3	0.0447	8.36
4	0.069	16.7
5	0.088	25.2
6	0.11	46
7	0.142	100
8	0.186	126

7. Strain rate $\frac{0.2}{2.5}$ / mt.

<u>S. No.</u>	<u>Pre-Strain</u>	<u>Stored energy x 10 ergs/cm³</u>
1	0.009	35
2	0.126	50
3	0.164	67
4	0.210	117
5	0.215	126
6	0.308	142
7	0.367	250

8. Strain rate $\frac{0.3}{2.5}$ / mt.

<u>S. No.</u>	<u>Pre-Strain</u>	<u>Stored energy x 10 ergs/cm³</u>
1	0.0742	12.54
2	0.130	50.06
3	0.144	113.0
4	0.178	150.0
5	0.215	176.0
6	0.26	180.0
7	0.296	263.0
8	0.340	237.5

Results of the Tensile Test for the Alloy

1. Strain rate $\frac{0.05}{2.5}$ / mt.

<u>S. No.</u>	<u>Pre-Strain</u>	<u>Stored energy</u> <u>$\times 10^6$ ergs/cm³</u>
1	0.0130	2.767
2	0.0199	3.409
3	0.026	3.57
4	0.038	5.21
5	0.0475	4.55
6	0.054	5.35

2. Strain rate $\frac{0.05}{2.5}$ / mt.

<u>S. No.</u>	<u>Pre-Strain</u>	<u>Stored energy</u> <u>$\times 10^6$ ergs/cm³</u>
1	0.00895	1.445
2	0.0186	2.249
3	0.047	2.704
4	0.0592	2.490
5	0.07	3.294
6	0.0862	3.480
7	0.1005	3.370
8	0.1060	3.453

3. Strain rate $\frac{0.05}{2.5}$ / mt.

<u>S. No.</u>	<u>Pre-Strain</u>	<u>Stored energy</u> <u>$\times 10^6$ ergs/cm³</u>
1	0.0256	1.963
2	0.0325	3.167
3	0.049	2.633
4	0.057	3.704
5	0.063	4.640
6	0.0764	4.65
7	0.0847	4.66
8	0.1060	4.8

Appendix B

Activation Energy Measurement for Copper

$$\text{Strain rate} = \frac{0.05}{2.5} / \text{mt.}$$

1. Temperature 160° C

<u>Pre-Strain</u>	<u>$\ln \frac{\Delta E}{KT}$</u>
0.0765	18.73
0.1102	18.91
0.140	19.024
0.172	19.18
0.196	19.25

3. Temperature 243° C

<u>Pre-Strain</u>	<u>$\ln \frac{\Delta E}{KT}$</u>
0.091	18.675
0.102	18.84
0.132	18.85
0.174	19.015
0.202	19.15
0.22	19.27
0.245	19.3

2. Temperature 223° C

<u>Pre-Strain</u>	<u>$\ln \frac{\Delta E}{KT}$</u>
0.062	18.71
0.088	18.6
0.106	18.83
0.125	18.890
0.167	18.984
0.223	19.096
0.237	19.19

4. Temperature 273° C

<u>Pre-Strain</u>	<u>$\ln \frac{\Delta E}{KT}$</u>
0.103	18.63
0.120	18.74
0.144	18.85
0.174	19.015
0.202	19.145
0.228	19.31
0.246	19.3

Activation Energy Measurements for the Alloy

$$\text{Strain rate} = \frac{0.05}{2.5} / \text{mt.}$$

1. Temperature 160° C

<u>Pre-Strain</u>	<u>$\ln \frac{\Delta E}{KT}$</u>
0.026	24.8
0.044	25.5
0.056	25.4
0.08	26
0.014	26.45
0.116	26.5

3. Temperature 243° C

<u>Pre-Strain</u>	<u>$\ln \frac{\Delta E}{KT}$</u>
0.044	18.4
0.051	18.9
0.07	19.35
0.082	19.25
0.09	20.1
0.118	20.8
0.131	21.75
0.162	22.4

2. Temperature 223° C

<u>Pre-Strain</u>	<u>$\ln \frac{\Delta E}{KT}$</u>
0.046	20.85
0.063	21.15
0.078	20.9
0.086	22.2
0.11	22
0.132	22.45

4. Temperature 300° C

<u>Pre-Strain</u>	<u>$\ln \frac{\Delta E}{KT}$</u>
0.045	17.4
0.063	17.6
0.076	18.3
0.104	18.9
0.131	19.02
0.15	19.3
0.163	19.6

VI. BIBLIOGRAPHY

1. G. E. Dieter, Mechanical Metallurgy, McGraw-Hill Book Co., 1961.
2. A. S. Nowick, Prog. Metal Physics, Vol. 4, 1, 1953.
3. H. L. Caswell, J. Appl. Physics, Vol. 29, 1210, 1958.
4. A. S. Nowick, Carnegie Inst. of Tech. Symp. on the Plastic Deformation of Crystalline Solids, 1950.
5. D. H. Niblett and J. Wilk, Advances in Phy., Vol. 9, 1960.
6. J. S. Koehler, Imperfections in Nearly Perfect Crystals, (Wiley), Ch. 7, p. 197, 1952.
7. A. Granato and K. Lucke, J. Appl. Phy., Vol. 27, 583, 1956.
8. C. A. Wert, J. Appl. Physics, Vol. 20, 29, 1949.
9. R. H. Chambers and R. Smolychowski, Physical Review, Vol. 117, 725, 1960.
10. D. N. Beshers, J. Appl. Physics, Vol. 30, 252, 1959.
11. A. Granato and K. Lucke, J. Appl. Physics, Vol. 27, 789, 1956.
12. T. A. Read, Trans. AIME, Vol. 143, 30, 1941.
13. A. S. Nowick, Phys. Review, Vol. 80, 249, 1950.
14. A. H. Cottrell, Dislocations in Plastic Flow in Crystals, (Oxford), 1953.
15. L. A. Kametsky, Thesis. Cornell University AFOSR-TN-56, 425.
16. W. P. Mason, J. Acoust. Soc. Amer., Vol. 19, 464, 1956.
17. G. S. Baker, J. Appl. Physics, Vol. 28, 734, 1957.
18. Reed-Hill, et al., Trans. AIME, Vol. 233, 1776, 1966.

19. Handbook of Chemistry and Physics, 45-edition, 1964.
20. H. K. Birnbaum and M. Levy, *Acta Met.*, 4, 84, 1956.
21. P. B. Hirsh, *Phil. Mag.*, Vol. 7, 67, 1962.

[illegible]

ME-1967-M-SAD-LOW